Mathematical Biosciences and Engineering

MBE, 17(1): 776–788.
DOI: 10.3934/mbe.2020040
Received: 29 April 2019
Accepted: 7 October 2019
Published: 31 October 2019

http://www.aimspress.com/journal/MBE

Research article

An automatic measurement method of spinal curvature on ultrasound coronal images in adolescent idiopathic scoliosis

Wei-wei Jiang[1], Xin-xin Zhong[1], Guang-quan Zhou[2], Qiu Guan[1], Yong-ping Zheng[3] and Sheng-yong Chen[1,4,*]

[1] College of Computer Science & Technology, Zhejiang University of Technology, Hangzhou 310014, China
[2] State Key Laboratory of Bioelectronics, School of Biological Science and Medical Engineering, Southeast University, Nanjing 210009, China
[3] Interdisciplinary Division of Biomedical Engineering, The Hong Kong Polytechnic University, Kowloon, Hong Kong 999077, China
[4] School of Computer Science and Engineering, Tianjin University of Technology, Tianjin 300384, China

* **Correspondence:** Email: sy@ieee.org; Tel/Fax: +8657185290085.

Abstract: This study proposed a new automatic measurement method of spinal curvature on ultrasound coronal images in adolescent idiopathic scoliosis (AIS). After preprocessing of Gaussian enhancement, the symmetric information of the image was extracted using the phase congruency. Then bony features were segmented from the soft tissues and background using the greyscale polarity. The morphological methods of image erosion and top-bottom-hat transformation, and geometric moment were utilized to identify the spinous column profile from the transverse processes. Finally, the spine deformity curve was obtained using robust regression. In-vivo experiments based on AIS patients were performed to evaluate the performance of the developed method. The comparison results revealed there was a significant correlation ($y = 0.81x$, $r = 0.86$) and good agreement between the new automatic method and the manual measurement method. It can be expected that this novel method may help to provide effective and objective deformity assessment method during the ultrasound scanning for AIS patients.

Keywords: automatic measurement; scoliosis; ultrasound; segmentation; phase congruency

1. Introduction

Scoliosis is defined as a three-dimensional torsional deformity of the spine and trunk, which causes a lateral curvature, an axial rotation and a disturbance of the sagittal plane normal curvatures, lordosis and kyphosis [1,2]. Adolescent idiopathic scoliosis (AIS) is the most prevalent form of scoliosis with the prevalence of 3–4% of kids in Hong Kong [3] and about 5% in China [4]. AIS occurs predominantly during puberty [5]. Patients are generally skeletally immature and at risk of curve progression during rapid growth. Regular monitoring is operating on this premise for early detection and further intervention [6].

The standing radiograph has been widely used to identify the spine deformity and is the current gold standard for AIS evaluation [7,8]. However, repeated radiographic monitoring causes X-ray exposure cumulation, which may increase the risk of cancer development, especially for children [9–11]. Presciutti et al. analyzed the radiation exposure for AIS patients and suggested to research newer imaging methods with limited ionizing radiation [12].

Compared with X-ray, ultrasound is a radiation-free imaging method. In addition, it is cost-effective and real-time. 2-D ultrasound is initially used to investigate the vertebral rotation and asymmetry of paraspinal muscle size [13,14]. Recently, freehand 3-D ultrasound, allowing viewing body anatomy in 3-D space, has been advanced by combining conventional 1-D array ultrasound probe with position sensor [15–21], and a number of such systems have been developed dedicated for scoliosis evaluation [19–21]. However, these methods are relatively time-consuming and subjectively because required sonographic landmarks are manually identified from dozens of continuous ultrasound images. To solve this problem, our group has developed a volume projection imaging (VPI) method to provide spine coronal image [22]. The principle of this study was to generate the ultrasound spine image using the shadow below the spinous processes on 2-D raw images. On the basis of the captured data sequence, a 3-D spine volume was firstly reconstructed. The coronal images (Figure 1a) were then obtained from the 3-D volume [23].

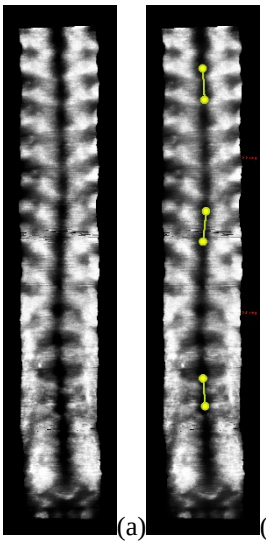

Figure 1. The ultrasound image generated by VPI method. (a) Original VPI image; (b) image with measurement result.

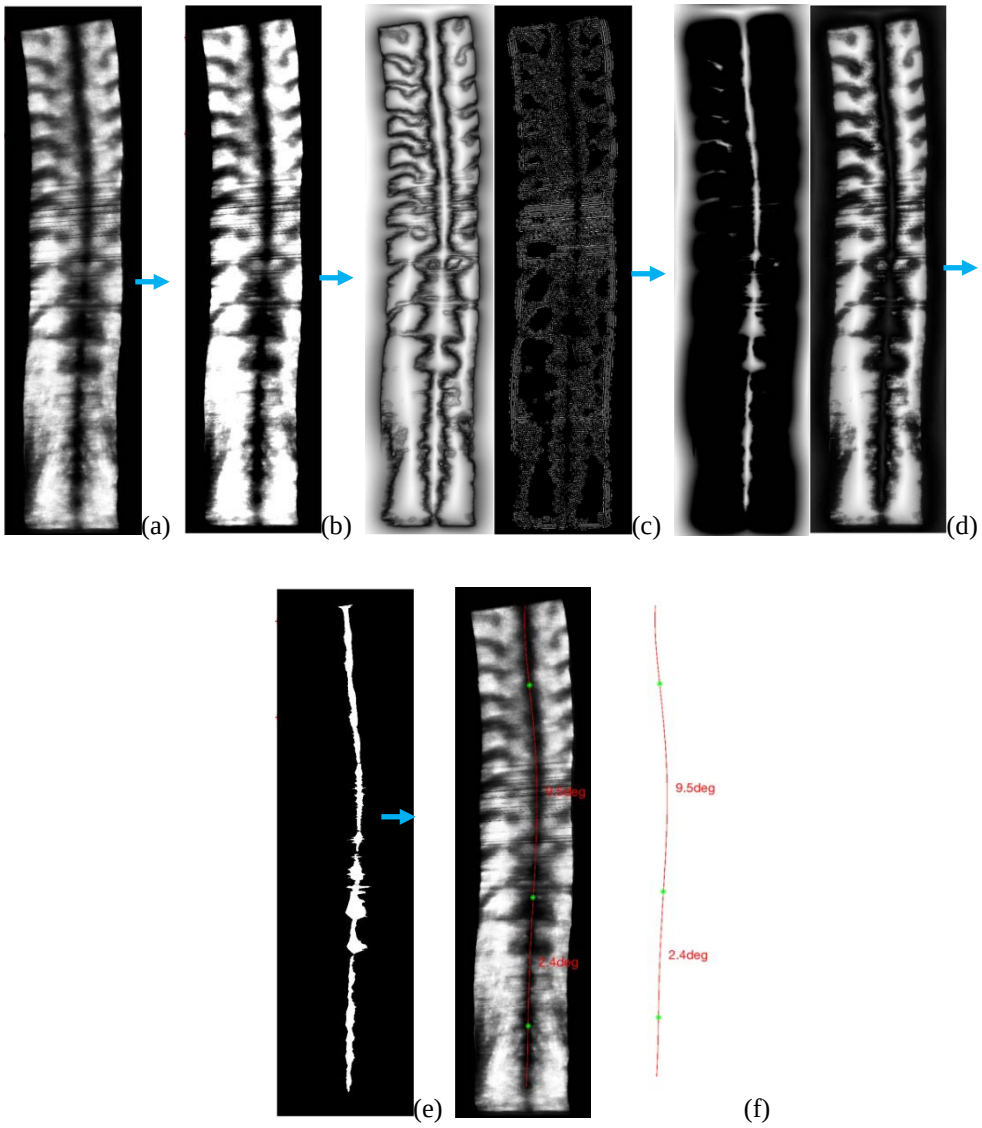

Figure 2. The flow diagram of the proposed automatic measurement method. (a) Original VPI image; (b) image after Gaussian enhancement; (c) symmetric information extraction with phase congruency; (d) bony segmentation with greyscale polarity; (e) identify of spinous column profile; (f) spine curvature calculation.

In clinics, Cobb angle was adopted to quantitatively indicate the spine deformity, which identifies the most tilted vertebrae on X-ray images and calculate the angle between two marked lines [7]. For the ultrasound coronal image generated by our VPI approach, a measurement method named VPI-SP was proposed [22]. This method uses spinous profile as reference, which generate an ultrasound shadow on the coronal image, as shown in Figure 1a. The portions containing curve inflection point is treated as the most tilted vertebrae and two short lines were manually marked to denote the location of the curve inflection point. The angle between two lines was calculated as the deformity angle (Figure 1b). Clinical tests based on 69 AIS patients were performed to compare the measurement results between VPI-SP method and the Cobb angle. It was reported that the proposed method could provide promising measurement [5]. Though the manual measurement method can provide effective assessment, the measurement is affected by the experience and knowledge of the

observer [24]. Studies presented that the intra-observer variation of measurement is about 2–3 degrees [22,25]. Therefore, the manual measurement method is subjective and tedious.

Accordingly, this study aims to develop an automatic measurement method of spinal curvature based on the ultrasound VPI image to quantitatively assess the spine deformity for AIS patients. In the following sections, this method is described in details. In vivo experiment is given to present the performance of the developed automatic method. The comparison between the proposed method and the manual method is also demonstrated.

2. Methods

2.1. The automatic measurement method of spinal curvature

The flow diagram of the proposed automatic measurement method is shown in Figure 2. This method consists of five steps: Image enhancement, symmetric information extraction with phase congruency, bony feature segmentation with greyscale polarity, identification of spinous column profile and spine curvature calculation.

2.1.1. Image enhancement

The reconstructed coronal image of spine using the VPI method is shown in Figure 2a. The black line lying nearby the midline is the spinous column profile which is used to calculate the spine deformity. Before segmentation, preprocessing was performed to improve the image enhancement and the conventional Gaussian enhancement method was used. As shown in Figure 2b, after preprocessing, the contrast of image was improved.

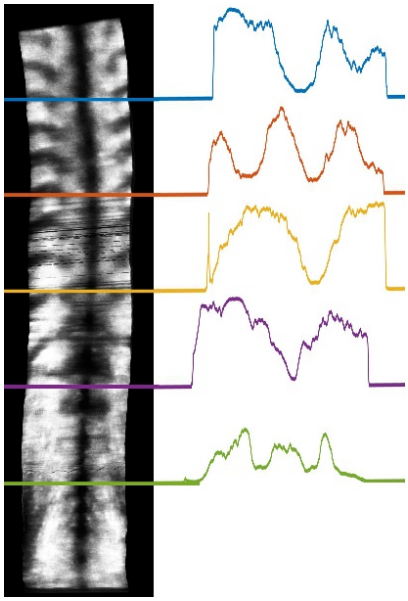

Figure 3. Scanline profiles which represent the intensity distribution (row numbers are at 400, 800, 1200, 1600, 2000).

2.1.2. Symmetric information extraction with phase congruency

Figure 3 shows the pixel intensity of one row on VPI image. The pixel intensity distribution is a valley-like curve in each row. The bottom of valley is the position of spinous process and this curve present an axis of local symmetry. As the Fourier series at points of symmetry is either at minima or maxima of their cycle, symmetry and asymmetry in image intensity can be extracted using phase congruency. Therefore, phase congruency can be used to detect the valley-like spinous profile [24]. Researchers have reported different approaches to calculate the phase congruency [26–28]. The method using log Gabor wavelet is a common choice, which can achieve feature localization with effective noise compensation [28]. The symmetric phase measurement at each point of the image can be calculated as follows:

$$PhaSy = \frac{SysEner - T}{\sum_1^{nscal} A + \varepsilon} = \frac{\sum_1^{nscal} \left[\sqrt{(\sum_M \sum_N Lg_t * Lp_{rs} * F_{img} * e_{MN})^2} + SysEner_{t-1} - \sqrt{H_t} \right] - T}{\sum_1^{nscal} A + \varepsilon} \quad (1)$$

$$LogG = e^{\frac{-(\ln(\frac{F_{1,1}}{f_r}))^2}{2*|\ln(sig_{sp}/fc)|^2}} \quad (2)$$

where Lg_t denotes a wavelet filter with scale t. Lp_{rs} denotes a low-pass filter with radius Rand sharpness s. F_{img} represents the phase-amplitude diagram after Fourier transform. To compute the bandpass image in the spatial domain, the inverse 2-D Fourier transform is used. e_{MN} represents the complex variable function. $SysEner_{t-1}$ is the cumulative sum of the previous symmetric energy. When $t - 1 = 0$, the symmetric energy is 0. H_t denotes the cumulative sum of the amplitudes of the genetic filter when the scale is t. The Log Gabor scale was set to 5 in this study.

After the processing of phase congruency, symmetry and asymmetry maps of the original image can be obtained, as shown in Figure 4.

2.1.3. Bony segmentation with greyscale polarity

The VPI image includes three parts: Background, soft tissues and bony features. It is noticed that the three parts are all bright in the symmetry phase map (Figure 4b). Actually, during the calculation of symmetry phase, we find the bony features have different greyscale polarity from the other two parts. Therefore, we further calculate the polarity of the symmetry features to segment the bony features using the following equations:

The positive polarity calculation equation:

$$PhaSy_1 =$$

$$\frac{SysEner - T}{\sum_1^{nscal} A + \varepsilon} = \frac{\sum_1^{nscal}\left[\sum_M \sum_N Lg_t * Lp_{rs} * F_{img} * e_{MN} + SysEner_{t-1} - \sqrt{H_t}\right] - T}{\sum_1^{nscal} A + \varepsilon} \tag{3}$$

The negative polarity calculation equation:

$$PhaSy_{-1} =$$

$$\frac{SysEner - T}{\sum_1^{nscal} A + \varepsilon} = \frac{\sum_1^{nscal}\left[-\left(\sum_M \sum_N Lg_t * Lp_{rs} * F_{img} * e_{MN}\right) + SysEner_{t-1} - \sqrt{H_t}\right] - T}{\sum_1^{nscal} A + \varepsilon} \tag{4}$$

where Eq (3) is used to calculate the positive value of the, which is the positive phase. And Eq (4) is to calculate negatively the value of the spatial bandpass map, which is the negative phase.

Figure 5 shows the polarity detection result which includes the positive and negative polarity detection images. From the negative polarity result, it can be noticed the bony features are segmented from the other two parts.

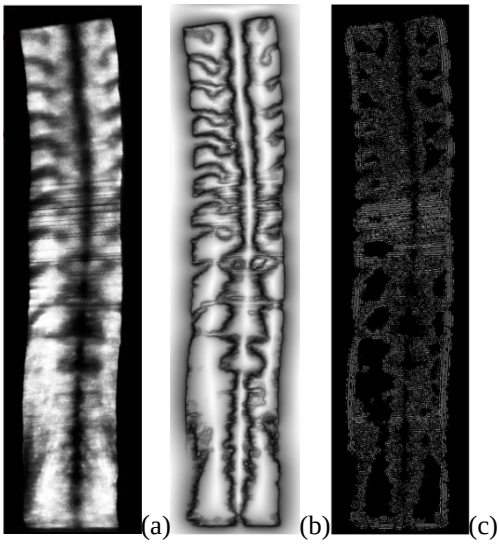

Figure 4. Symmetric information extraction with phase congruency. (a) Original image; (b) the symmetry phase of the image; (c) the asymmetry phase of the image.

2.1.4. Identification of spinous column profile

The segmented bony features (Figure 5b) contain the spinous column profile and the transverse processes. This step is to identify the spinous column profile according to the image of negative polarity detection.

The flowchart of this step is illustrated by Figure 6. The conventional image erosion method was firstly used to remove the contour lines of the image (Figure 6b). Then we use the morphological method of top-bottom-hat transformation to adjust the image brightness and feature quality (Figure 6c). In this image, the discrete areas of spinous processes and transverse processes were presented. To separate the continuous spinous column profile, the connected

components and geometric moment were adopted. The geometric moment was calculated according to the following equation:

$$M_{ij} = \sum_{R}\sum_{C}(x)^i * (y)^j * F(x,y) \tag{5}$$

where ij represents the $i+j$ moment, R and C represent the row and column, respectively. $F(x,y)$ denotes the gray value at coordinate of (x,y). The center and direction of the object are calculated by using the mixed center moment.

The centroid calculation equation:

$$x_c = \frac{M_{10}}{M_{00}}; y = \frac{M_{01}}{M_{00}} \tag{6}$$

The orientation angle was calculated as follows:

$$\theta = \frac{1}{2} arctan\left(\frac{2\left(\frac{M_{11}}{M_{00}} - x_c * y_c\right)}{\frac{M_{11}}{M_{00}} - x_c^2 - \frac{M_{02}}{M_{00}} - y_c^2}\right) \tag{7}$$

The continuous area of spinous column profile is shown in Figure 5d.

2.1.5. The spine deformity angle measurement

Based on the above area of spinous column profile, we calculate the median value of each row as the profile line. However, it's found there is some pixel missed, as shown in Figure 7. To solve this problem, we use robust linear regression over each window. The spine curvature measurement result is shown in Figure 8.

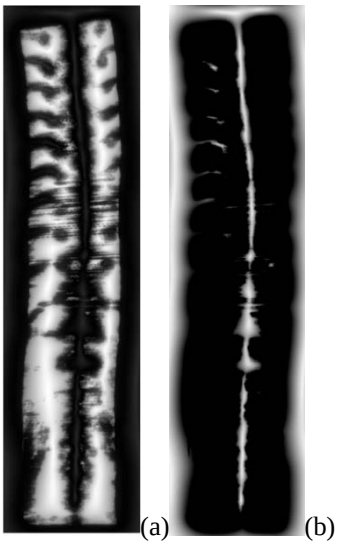

Figure 5. The bony features segmentation. (a) The image of positive polarity detection; (b) the image of negative polarity detection.

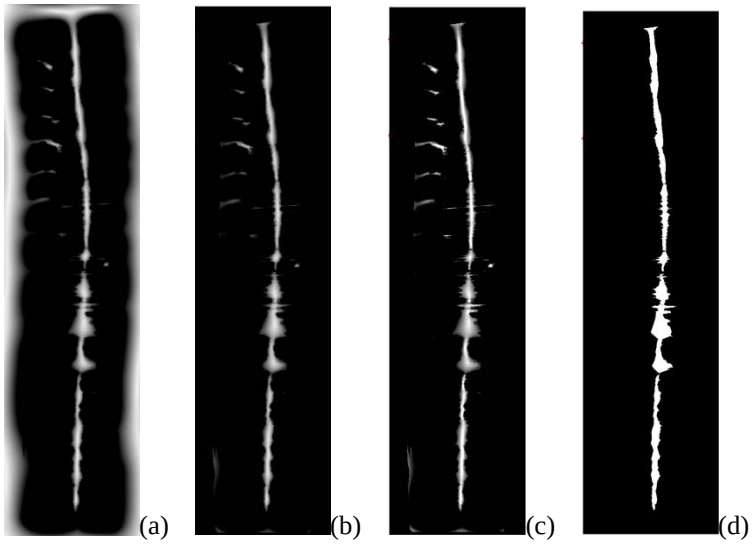

Figure 6. Identification of spinous column profile. (a) The image of spinous column profile and transverse processes; (b) remove contour lines using image erosion; (c) adjust the image brightness with top-bottom-hat transformation; (d) calculate the continuous area of spinous column profile using connected components and geometric moment.

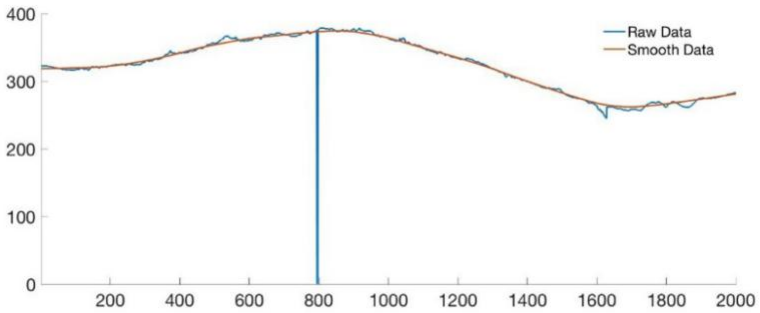

Figure 7. Data smooth with robust linear regression over each window length.

2.2. Experiments

In vivo experiments were performed to evaluate the performance of the developed automatic measurement method. This study was approved by the local institutional review board. All participants (or parents for the participants under 18 years old) provided written informed consent for participation in the study. In total, 111 patients with AIS (mean age: 16.2 ± standard deviation (SD) 3.9 years; BMI: 18.7 ± 3.0 kg/m^2) were recruited. The exclusion criteria were: (1) patients with metallic implants; (2) patients who had received brace or surgical treatment; (3) patients with BMI index higher than 25.0 kg/m^2.

In the test, each subject was scanned by the same operator using the Scolioscan system which was developed on the basis of 3D ultrasound imaging [5,8]. The acquired ultrasound images and corresponding spatial data were reconstructed to generate VPI images. Based on the obtained VPI images, an observer who was experienced in ultrasound imaging of scoliosis measured the deformity

angle using the aforementioned manual measurement method. Then this VPI image was measured again using the developed automatic assessment method.

For the comparison study, the deformity angles measured by the manual method and the automatic method were compared. A linear regression analysis with zero intercept and with intercept were described. The Pearson correlation coefficient r was calculated to evaluate the correlation of the two methods. All statistical analyses were conducted using the statistical software (SPSS for Windows, version 17.0; SPSS, Chicago, IL, USA). The agreement of the two methods were also investigated using the Bland and Altman's method. A P value of less than 0.05 was accepted as level of significance.

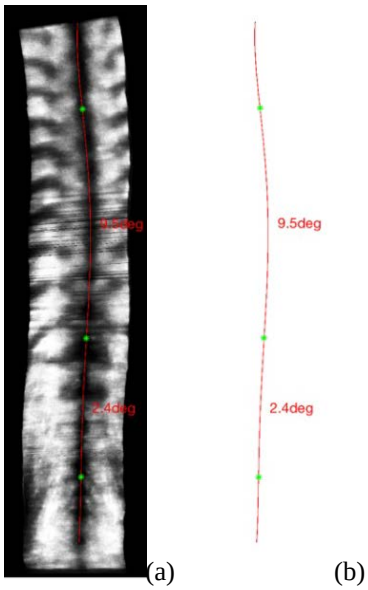

(a) (b)

Figure 8. Spine deformity angle calculation. (a) The spine deformity curvature on VPI image; (b) the spine deformity curvature. Red curve is the estimated spine curve and the green point is inflection point. We fit the spine curve with 6th order polynomial.

3. Results

For each subject, two measurement images were produced using the manual measurement method and the automatic measurement method. Figure 9 presents two typical images from the same subject using the two measurement methods. Figure 9a is the comparison of the manual method and the automatic method, and Figure 9b is the automatic method. As shown in Figure 9a, the lines of the two methods could both locate positions of infection points. However, for the manual method, the marked straight lines could not exactly coincide with the tangent lines at the corresponding inflection point, which could cause measurement errors.

The mean deformity angles for the automatic measurement method and the manual method were 10.2 and 12.5 degrees, respectively. As illustrated in Figure 10a, a significant correlation was investigated between the manual method and the automatic method (with zero intercept: $y = 0.81x$, $r = 0.86$; with intercept: $y = 0.77x + 0.52$, $R = 0.74$). The Bland-Altman plot (Figure 10b) shows a low mean difference ($D = -2.3$ degrees), mean absolute difference (MAD = 2.3 degrees) and the

differences symmetrically distributed around the mean difference (±1.96 SD = 6.2 degrees). Therefore, there was a good agreement between the measurement results of the two methods.

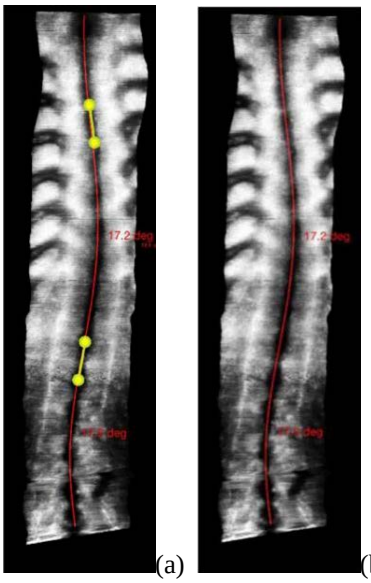

(a) (b)

Figure 9. An example of spine curvature measurement using the manual measurement method and the developed automatic method. (a) Comparison image with both two measurement methods; (b) image with automatic measurement.

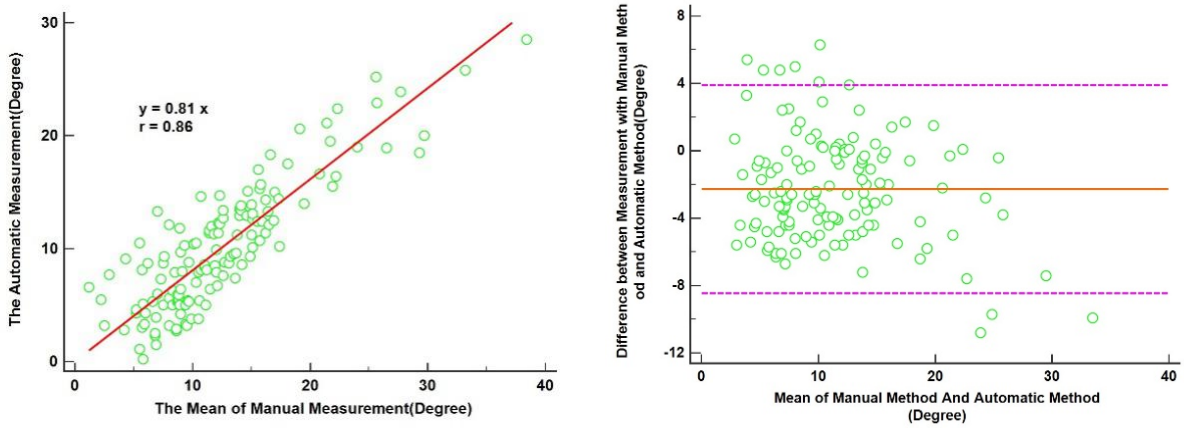

(a) (b)

Figure 10. The comparison results between manual measurement method and the developed automatic method. (a) The correlation between angles measured by the two methods; (b) bland-Altman plot of angles measured by the two methods.

4. Conclusions

We presented an automatic measurement method of spinal curvature on ultrasound coronal

images of AIS patients. After preprocessing of Gaussian enhancement, the symmetric information of the image was extracted using the phase congruency. Then the greyscale polarity was performed to segment the bony features from the soft tissues and background. The morphological methods of image erosion and top-bottom-hat transformation, and geometric moment were utilized to identify the spinous column profile from the transverse processes. Finally, the spine deformity curve was obtained using robust linear regression. Compared with the previously reported segmentation method [24], the polarity of phase was calculated in this method, which can be used to segment the bony features from the soft tissue regions.

In vivo experiments based on AIS patients were performed to evaluate the performance of the newly developed automatic measurement method. The comparison results revealed there were significant correlation and good agreement between the new automatic method and the manual measurement method. It can be expected that this novel method may help to provide effective and objective deformity assessment method during the ultrasound scanning for AIS patients. In the future, large-scale clinical tests will be conducted to further demonstrate the potential of this automatic method.

Acknowledgements

This study was supported by the National Natural Science Foundation of China (61701442, U1509207, 61771130), the Natural Science Foundation of Zhejiang Province (LY18F030025, LSD19H180003).

Conflict of interest

The authors declare no competing interests.

References

1. S. L. Weinstein, L. A. Dolan, J. G. Wright, et al., Effects of bracing in adolescents with idiopathic scoliosis, *N. Engl. J. Med.*, **369** (2013), 1512–1521.
2. W. W. Jiang, C. L. K. Cheng, J. P. Y. Cheung, et al., Patterns of coronal curve changes in forward bending posture: A 3D ultrasound study of adolescent idiopathic scoliosis patients, *Eur. Spine J.*, **27** (2018), 2139–2147.
3. D. Y. T. Fong, K. M. C. Cheung, Y. W. Wong, et al., A population-based cohort study of 94401 children followed for 10 years exhibits sustained effectiveness of scoliosis screening, *Spine J.*, **15** (2015), 825–833.
4. H. Fan, Z. Huang, Q. Wang, et al., Prevalence of idiopathic scoliosis in Chinese schoolchildren, *Spine*, **41** (2016), 259–264.
5. Y. P. Zheng, T. T. Y. Lee, K. L. Lai, et al., A reliability and validity study for Scolioscan: A radiation-free scoliosis assessment system using 3D ultrasound imaging, *Scoliosis Spinal Disord.*, **13** (2016), 13.
6. M. Thomsen and R. Abel, Imaging in scoliosis from the orthopaedic surgeon's point of view, *Eur. J. Radiol.*, **58** (2006), 41–47.
7. J. Cobb, Outline for the study of scoliosis, *Orthop. Surg. Instr. Course Lect. AAOS*, **5** (1948), 261–275.

8. C. W. J. Cheung, G. Q. Zhou, S. Y. Law, et al., Freehand three-dimensional ultrasound system for assessment of scoliosis, *J. Orthop. Transl.*, **3** (2015), 123–133.
9. A. R. Levy, M. S. Goldberg, N. E. Mayo, et al., Reducing the lifetime risk of cancer from spinal radiographs among people with adolescent idiopathic scoliosis, *Spine*, **21** (1996), 1540–1547.
10. C. M. Ronckers, C. E. Land, J. S. Miller, et al., Cancer mortality among women frequently exposed to radiographic exams for spinal disorders, *Radiat. Res.*, **174** (2010), 83–90.
11. I. Schmitz-Feuerhake and S. Pflugbeil, 'Lifestyle' and cancer rates in former East and West Germany: The possible contribution of diagnostic radiation exposures, *Radiat. Prot. Dosimetry*, **147** (2011), 310–313.
12. S. M. Presciutti, T. Karukanda and M. Lee, Management decisions for adolescent idiopathic scoliosis significantly affect patient radiatin exposure, *Spine J.*, **14** (2014), 1984–1990.
13. S. Suzuki, T. Yamamuro, J. Shikata, et al., Ultrasound measurement of vertebral rotation in idiopathic scoliosis, *J. Bone Jt. Surg.*, **71** (1989), 252–255.
14. K. P. Kennelly and M. J. Stokes, Pattern of asymmetry of paraspinal muscle size in adolescent idiopathic scoliosis examined by real-time ultrasound imaging. A preliminary study, *Spine*, **18** (1993), 913–917.
15. Q. H. Huang, J. L. Lan and X. L. Li, Robotic arm based automatic ultrasound scanning for three-dimensional imaging, *IEEE. Trans. Ind. Inform*, **15** (2019), 1173–1182.
16. Q. H. Huang, B. W. Wu, J. L. Lan, et al., Fully automatic three-dimensional ultrasound imaging based on conventional B-scan, *IEEE. Trans. Biomed. Circ. Syst.*, **12** (2018), 426–436.
17. Q. H. Huang, Z. Z. Zeng and X. L. Li, 2.5-Dimensional Extended Field-of-View Ultrasound, *IEEE Trans. Med. Imaging.*, **37** (2018), 851–859.
18. Q. H. Huang and Z. Z. Zeng, A review on real-time 3D ultrasound imaging technology, *Biomed. Res. Int.*, **2017** (2017), 1–20.
19. W. Chen, E. H. M. Lou and L. H. Le, *Using ultrasound imaging to identify landmarks in vertebra models to assess spinal deformity*, 2011 Annual International Conference of the IEEE Engineering in Medicine and Biology Society, 8495–8498. Available from: https://ieeexplore_ieee.gg363.site/abstract/document/6092096.
20. Q. H. Huang, Q. F. Deng, L. Li, et al., Scoliotic imaging with a novel double-sweep 2.5-dimensional extended field-of-view ultrasound, *IEEE Trans. Ultrason. Ferroelectr. Freq. Control*, **8** (2019), 1304–1315.
21. T. Ungi, F. King, M. Kempston, et al., Spinal curvature measurement by tracked ultrasound snapshots, *Ultrasound Med. Biol.*, **40** (2014), 447–454.
22. C. W. J. Cheung, G. Q. Zhou, S. Y. Law, et al., Ultrasound volume projection imaging for assessment of scoliosis, *IEEE Trans. Med. Imaging*, **34** (2015), 1760–1768.
23. W. W. Jiang, G. Q. Zhou, K. L. Lai, et al., A fast 3-D ultrasound projection imaging method for scoliosis assessment, *Math. Biosci. Eng.*, **16** (2019), 1067–1081.
24. G. Q. Zhou, W. W. Jiang, K. L. Lai, et al., Automatic measurement of spine curvature on 3-D ultrasound volume projection image with phase features, *IEEE Trans. Med. Imaging*, **36** (2017), 1250–1262.
25. M. Young, D. L. Hill, R. Zheng, et al., Reliability and accuracy of ultrasound measurements with and without the aid of previous radiographs in adolescent idiopathic scoliosis (AIS), *Eur. Spine J.*, **24** (2015), 1427–1433.

26. M. Felsberg and G. Sommer, The monogenic signal, *IEEE Trans. Signal Process.*, **49** (2001), 3136–3144.
27. L. Zhang, L. Zhang, X. Q. Mou, et al., FSIM, A Feature Similarity Index for Image Quality Assessment, *IEEE Trans. Image Process.*, **20** (2011), 2378–2386.
28. P. Kovesi, Phase congruency: A low-level image invariant, *Psychol. Res.*, **64** (2000), 136–148.

AIMS Press